Retrieval of Surface Reflectance and Estimation of Forest Leaf Area Index (LAI) Using Hyperion, ALI, and AVIRIS

Peng Gong, Greg Biging, and R. Pu

Objectives

The objectives of this investigation were to develop a simple atmospheric correction method; map leaf area index (LAI), study vegetation indices (VIs), and extract red edge optical parameter for estimating forest LAI with the EO-1 Advanced Land Imager (ALI) and Hyperion and with the Airborne Visible/Infrared Imaging Spectrometer (AVIRIS); examine the capabilities of the three sensors for extracting LAI information; and compare different VIs constructed from all possible Hyperion bands and red-edge parameters for LAI estimation.

Study Site and Datasets

Two study sites were used in Patagonia, Argentina, that were located in a flat, semiarid region. The study area had many patches of conifer forest plantations of different species of pine trees as well as some broad-leaf species and shrubs and grasses.

On March 27-29, 2001, field reflectance measurements were obtained for several targets using ASD Field Spec®Pro, and 70 LAI measurements were taken. On March 27, 2001, ALI and Hyperion measurements were acquired at a spatial resolution of 30 meters. AVIRIS data at a spatial resolution of 3.6 meters were acquired on February 15, 2001. Because of overcast conditions at one study site, data from only one of the two sites (the north site) were used for the analysis (Figure 1).
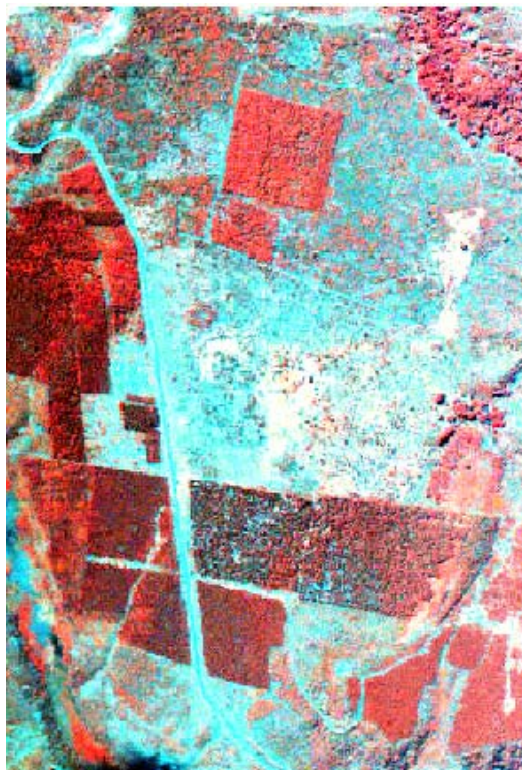

Figure 1. Part of the AVRIS image over the selected study site in Patagonia, Argentina.
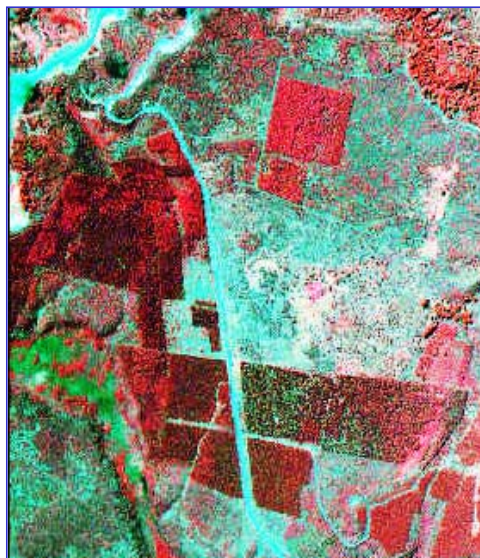
Atmospheric Correction and LAI Mapping
Atmospheric correction was obtained by means of a radiative transfer model. The model was applied to sensor data in which three total radiances were simulated using MODTRAN4 to obtain improved pixel-based surface reflectance. Ground spectrometer data were also used to modify the retrieved surface reflectance images.

Using the improved retrieved surface reflectance images from the ALI, Hyperion, and AVIRIS sensors, LAI was estimated and mapped by following a set of procedures that involved extracting pixel values at 32 LAI measured plots, performing general correlation analysis of spectral bands with LAIs, and performing regression analysis on six bands selected from the total number of bands available for each sensor. Results were compared using only data from these six bands for each sensor.

The effectiveness of the procedures was evaluated using the following criteria:
1. Multi-correlation coefficient, R^2, of the LAI prediction model.
2. Overall average accuracy of LAI prediction accuracy of training and test samples.
3. Visual examination of LAI maps.

Results indicated that AVIRIS had the highest correlation with LAI among the three sensors. Hyperion had the next highest correlation, and ALI had the lowest correlation. Figure 2 shows a pseudo-color composite from AVIRIS (upper left) and LAI maps for the three sensors. AVIRIS data experienced fewer atmospheric effects than the data from the other sensors, especially in the visible and near infrared (VNIR) region. Hyperion was especially problematic in this region because of its strong atmospheric scattering.

		LAI
		0 – 1
		1 – 2
		2 – 3
		3 – 4
		4 – 5
		> 5

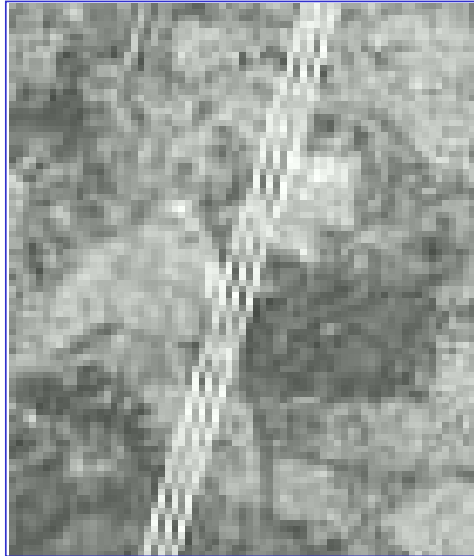**Pseudo color composite of AVIRIS.**   **LAI map from AVIRIS.**
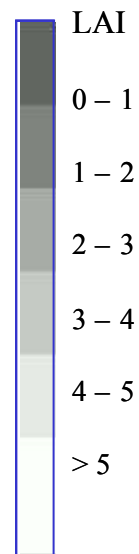
LAI map from Hyperion

LAI map from ALI. The three white lines were from three ALI dead detectors.

Figure 2. LAI maps.

Conclusions
Investigators concluded that atmospheric correction is critical for hyperspectral data applications, especially for measurements in the VNIR region. Results indicated that the method of atmospheric correction used in this study holds promise but needs refinement. Results further indicated that retrieval of surface reflectance was the most successful for AVIRIS, followed by Hyperion and lastly by ALI. Mapped LAI results demonstrated that the procedure used in this investigation to map LAI can produce reasonable LAI maps, and that the LAI map produced with AVIRIS data was more reliable than the maps produced with Hyperion and ALI, which appear to have similar capabilities for LAI mapping. Hyperion in particular seems to have more potential for applications in the shortwave infrared (SWIR) region than in the VNIR region because the atmospheric effects are more pronounced on VNIR measurements. For imagery in the SWIR region, if atmospheric correction is carefully conducted, Hyperion has the potential to produce results similar to that of AVIRIS.

Estimating Forest LAI Using Vegetation Indices Derived From Hyperion Hyperspectral Data

Method
Pixel-based retrieved reflectance spectra from calibrated Hyperion images at the 32 LAI measurement plots were extracted from the image. One to four homogenous pixels were extracted and averaged for each LAI plot. The 12 VIs (Table 1) were applied to any possible pair of the 168 Hyperion bands. Note that red (R) bands and near IR (NIR) bands used for constructing one VI in Table 1 have been extended to all 168 bands. Consequently, for each pair of bands there are 12 VIs for each of the 32 LAI measurements.

For each of the 12 VIs, a linear correlation coefficient (R^2) was calculated between the VI and LAI measurement (32 samples). Because most LAI measurements are less than 5 in this study, a

linear R^2 is a suitable indicator for finding some important bands contributing to better correlation between a two-band index and the LAI. Since each VI in Table 1 could be constructed from any pair among the possible 168 bands, a linear correlation coefficient (R^2) matrix could be constructed. From the correlation matrices, hyperspectral bands with high correlation coefficients were examined.

Conclusions

Results indicate that many hyperspectral bands in the SWIR region and some in the NIR region have the greatest potential to form indices for LAI estimation. The most effective band wavelengths are centered near 820, 1040, 1200, 1250, 1650, 2100, and 2260 nm with bandwidths ranging from 10 to 300 nm (Table 2). These bands are controlled by plant leaf water content, yet the absorption features by other biochemicals such as protein, nitrogen, lignin, cellulose, sugar, and starch, may have indirect impacts. VIs derived from the R and NIR bands did not produce as high correlations with LAI as those with bands in the SWIR and NIR regions. Based on their high correlation with LAI measurements, the Modified Non-Linear Vegetation Index (MNLI), Simple-Ratio Vegetation Index (SRVI), and Normalized Difference Vegetation Index (NDVI) were recommended for use in environments similar to this study site for LAI estimation using satellite-based hyperspectral data.

Extraction of Red Edge Optical Parameters from Hyperion Data for Estimation of Forest LAI

Method

A correlation analysis was conducted between forest LAI and two red edge parameters: red edge position (REP) and red well position (RWP), extracted from reflectance image retrieved from Hyperion data. Field spectrometer data and LAI measurements were collected on the same day as the EO-1 satellite overpassed the study site in the Patagonia region of Argentina. They were extracted with four approaches: 4-point interpolation, polynomial fitting, Lagrangian technique, and IG (inverted-Gaussian) modeling.

Table 1. Summary of 12 two-band vegetation indices used in this analysis.

Index	Formula	Description	References (e.g.)
SR	ρ_{NIR} / ρ_R	Near-infrared / Red reflectance ratio (Simple Ratio VI). Related to changes in amount of green biomass, pigment content and concentration and leaf water stress etc.	Baret and Guyot, 1991; Tucher, 1979.
NDVI	$(\rho_{NIR}-\rho_R)/(\rho_{NIR}+\rho_R)$	Normalized Difference Vegetation Index. Related to changes in amount of green biomass, pigment content and concentration and leaf water stress etc.	Fassnacht et al., 1997; Smith et al., 1991.
PVI	$\frac{1}{\sqrt{a^2+1}}(\rho_{NIR} - a\rho_R - b)$ a = slope of the soil line, b = soil line intercept	Perpendicular Vegetation Index, orthogonal to the soil line. Attempts to eliminate differences in soil background and is most effective under conditions of low LAI, applicable for arid and semiarid regions.	Baret and Guyot, 1991; Huete et al., 1985.
SAVI	$\frac{(\rho_{NIR} - \rho_R)(1+L)}{(\rho_{NIR} + \rho_R + L)}$ L = a correction factor	Soil Adjusted Vegetation Index. L ranges from 0 for very high vegetation cover to 1 for very low vegetation cover; minimizes soil brightness-induced variations. L=0.5 can reduce soil noise problems for a wide range of LAI.	Huete, 1988; Leeuwen and Huete, 1996.

Index	Formula	Description	References (e.g.)
NLI	$(\rho_{NIR}^2 - \rho_R)/(\rho_{NIR}^2 + \rho_R)$	Non-Linear vegetation Index. Considers that the relationship between many VIs and surface biophysical parameters is often nonlinear, and NLI linearizes relationships with surface parameters that tend to be nonlinear.	Goel and Qin, 1994
RDVI	$(\rho_{NIR} - \rho_R)/(\rho_{NIR} + \rho_R)^{1/2}$	Renormalized Difference Vegetation Index. RDVI linearizes relationships with surface parameters that tend to be nonlinear.	Roujean and Breon, 1995.
MSR	$\dfrac{(\rho_{NIR}/\rho_R - 1)}{(\rho_{NIR}/\rho_R)^{1/2} + 1}$	Modified Simple Ratio. It can be an improvement over RDVI for linearizing the relationships between the index and biophysical parameters.	Chen, 1996.
WDVI	$\rho_{NIR} - a\rho_R$ a = slope of the soil line	Weighted Difference Vegetation Index. WDVI assumes that the ratio between NIR and R reflectances of bare soil is constant; it is related to PVI, but it has an unrestricted range.	Clevers, 1988; Clevers, 1991.
MNLI	$\dfrac{(\rho_{NIR}^2 - \rho_R)(1+L)}{(\rho_{NIR}^2 + \rho_R + L)}$ L = a correction factor	Modified Non-linear vegetation Index. MNLI is an improved version of NLI. L=0.5 may be applicable for a wide range of LAI.	Developed in this paper.
NDVI*SR	$\dfrac{(\rho_{NIR}^2 - \rho_R)}{(\rho_{NIR} + \rho_R^2)}$	Attempts to combine merit of NDVI with that of SR.	Developed in this paper.
SAVI*SR	$\dfrac{(\rho_{NIR}^2 - \rho_R)}{(\rho_{NIR} + \rho_R + L)\rho_R}$	Attempts to combine merit of SAVI with that of SR.	Developed in this paper.
TSAVI	$\dfrac{a(\rho_{NIR} - a\rho_R - b)}{[a\rho_{NIR} + \rho_R - ab + X(1+a^2)]}$ a = slope of the soil line, b = soil line intercept, X = adjustment factor to minimize soil noise.	Transformed Soil Adjusted Vegetation Index. Modify Huete (1988) SAVI to compensate for soil variability due to changes in solar elevation and canopy structure.	Baret and Guyot, 1991;

Note: $\rho_R\ and\ \rho_{NIR}$ denoted as reflectances in red and near-infrared wavelengths, but in this study, they represent band 1 and band 2 across all avaliable 168 bands of Hyperion data.

Table 2. Potential hyperspectral bands for 12 vegetation indices applied to forest LAI estimation.

Index	R^2 NIR-R/Optim.	Band center (nm)	Bandwidth (nm)	Band description (spectral region and possible absorption features)
SR	0.55/0.70	825	140	NIR region, **cell structure** multi-reflected spectra.
		1038	230	NIR-SWIR region, **water**, **protein**, lignin, starch & oil absorption
		1250	180	SWIR region, **water**, cellulose, starch and lignin absorption
		1648	290	SWIR region, **protein**, **nitrogen**, **lignin**, **cellulose**, sugar, starch absorption.
NDVI	0.55/0.70	…	…	4 bands similar to SR's
PVI	0.45/0.64	814	140	NIR region, **cell structure** multi-reflected spectra.
		1050	100	NIR-SWIR region, **protein**, lignin, and oil absorption
		1250	190	SWIR region, **water**, cellulose, starch and lignin absorption
		2100	10	SWIR region, **starch,** cellulose absorption
SAVI	0.50/0.67	…	…	4 bands similar to NDVI's or SR's

Index	R² NIR-R/Optim.	Band center (nm)	Bandwidth (nm)	Band description (spectral region and possible absorption features)
NLI	0.50/0.73	821	157	NIR region, **cell structure** multi-reflected spectra.
		1200	578	NIR-SWIR region, **water**, protein, starch, lignin, cellulose, and oil absorption
		1250	191	SWIR region, **water**, cellulose, starch and lignin absorption
		1640	300	SWIR region, **protein**, **nitrogen**, **lignin**, **cellulose**, sugar, starch absorption.
RDVI	0.45/0.66	810	170	NIR region, **cell structure** multi-reflected spectra.
		1054	10	SWIR region, lignin and oil absorption
		1255	161	SWIR region, **water**, cellulose, starch and lignin absorption
		1669	10	SWIR region, lignin and starch absorption
		2093	10	SWIR region, starch and cellulose absorption
MSR	0.50/0.70	…	…	4 bands similar to NDVI's or SR's
WDVI	0.45/0.63	1639	10	SWIR region, non apparent absorption
		2113	10	SWIR region, **starch** and cellulose absorption
		2285	30	SWIR region, starch, cellulose and protein absorption
MNLI	0.45/0.75	…	…	4 bands similar to NLIs
NDVI*SR	0.50/0.71	…	…	4 bands similar to NDVI's or SR's, but
SAVI*SR	0.50/0.71	…	…	1 - 4 bands similar to SAVI's or SR's
		2083	30	SWIR region, sugar, starch and cellulose absorption
		2153	10	SWIR region, protein absorption
TSAVI	0.50/0.71	832	120	NIR region, **cell structure** multi-reflected spectra.
		1038	150	NIR-SWIR region, **water**, **protein**, lignin, starch & oil absorption
		1240	170	SWIR region, **water**, lignin, cellulose and starch absorption
		1660	260	SWIR region, **lignin**, **cellulose, sugar**, starch, protein, and nitrogen absorption
		2108	20	SWIR region, **starch**, cellulose and protein absorption

Note: Optim. = optimal correlation R²; **bold chemicals** are principal for the absorption features

Conclusions

The experimental results indicate that the 4-point approach is a more practical method for extracting the two red edge parameters because only 4 bands are needed. The polynomial fitting approach also has the advantage that it is a direct method for deriving these parameters. It also has practical value if hyperspectral data (spectral resolution narrower than 10 nm like Hyperion data) are available. Moreover, this approach can model the phenomenon of two maximum first-derivatives along the red edge curve. Since the first derivative spectra frequently are not directly available for most multi/hyperspectral sensors, use of the Lagrangian technique is less practical. The IG modeling, used for extracting red edge optical parameters from space-borne hyperspectral data, needs further testing if a linear fitting approach as tested in this study is applied.